Observation of Chiral Spin Fluctuations in Insulating Planar Cuprates

P. E. Sulewski, P. A. Fleury, K. B. Lyons, and S-W. Cheong
AT&T Bell Laboratories, Murray Hill, New Jersey 07974
(Received 29 August 1991)

A recent theory of Raman scattering in the Hubbard model predicts scattering of A_2 symmetry arising from chiral spin fluctuations. In the doped planar cuprates, chiral spin fluctuations have been speculated to play a central role in establishing the normal-state properties. In addition to spin fluctuation scattering in the B_1, A_1, and B_2 symmetries, we report here the direct observation of dynamic chiral spin fluctuations, appearing in the inelastically scattered light of A_2 symmetry. In Gd_2CuO_4, the A_2 scattering broadly peaks near 4700 cm^{-1} ($\sim 5J$) and extends beyond 8000 cm^{-1} (1 eV).

PACS numbers: 78.30.Hv, 75.30.Ds, 75.40.Gb, 75.50.Ee

A rather complete understanding of the dynamics of the spin degrees of freedom in the cuprates has been gained in the past few years through studies of inelastic light scattering over large (~ 1 eV) energy shifts [1–3]. The spin-pair scattering, observed in the B_1, A_1, and B_2 symmetry channels, has provided a quantitative picture of the quantum spin excitations in the two-dimensional (2D) spin-$\frac{1}{2}$ Heisenberg system.

Now, through experimental improvement and motivated by recent theoretical predictions [4], a new type of light scattering, of A_2 symmetry, has been observed in the layered cuprates. This scattering results from a term in the effective scattering Hamiltonian proportional to the spin chirality operator, $\sum \mathbf{S}_i \cdot (\mathbf{S}_j \times \mathbf{S}_k)$, and thus represents the spectrum of chiral spin fluctuations. In the doped cuprates, chiral spin fluctuations have been invoked to explain the normal-state properties [5–7], and Wen, Wilczek, and Lee [5] have shown that the elementary excitations of the chiral spin state obey fractional statistics. An ideal gas of particles obeying fractional statistics has been speculated to exhibit a superconducting ground state [8].

Since the spin chirality appears in the scattering Hamiltonian, Raman measurements provide a direct probe of dynamic chiral spin fluctuations in the cuprates. For the insulating cuprates, which exhibit antiferromagnetic ground states, the ground-state expectation value of the spin chirality vanishes. Nevertheless, as we will show, dynamic chiral spin fluctuations are expected and observed with inelastic light scattering. In order for the excitations which we observe in the insulating materials to relate to current theories of doped materials, some portion of their spectral weight must be transferred to a quasielastic line, with an extremely narrow width, well below 1 cm^{-1} [7]. The observation of such a narrow quasielastic line lies beyond the scope of the experiments presented here.

Our previous experiments [3,9] have shown quantitative similarities among the A_1, B_1, and B_2 components for the entire M_2CuO_4 series (M = La, Pr, Nd, Sm, Eu, Gd), demonstrating that these features are intrinsic to the CuO_2 planes. In this work we focus on the tetragonal materials [10] Gd_2CuO_4 and Pr_2CuO_4, where crystals with excellent surface quality have been grown. In these crystals, the observed intensity of the A_2 component is $\sim 50\%$ of that of the B_2 intensity. The A_2 contribution peaks at higher frequencies than scattering in the other symmetry channels, consistent with estimates from spin-wave theory.

The Gd_2CuO_4 and Pr_2CuO_4 single crystals are grown from a CuO flux, as has been previously described [10]. Each of the as-grown crystals exhibits at least one highly reflecting face, free of residual flux, and all spectra are taken from as-grown surfaces. The basal plane dimensions of the Gd_2CuO_4 and Pr_2CuO_4 crystals are 4×1.5 and 2×1.5 mm^2, respectively.

The spectra are obtained with 30 mW from an Ar-ion laser, focused to a line 0.1×1.5 mm^2 on the samples at room temperature. Two excitation wavelengths—4880 and 5145 Å—are used to discriminate against fluorescence contributions. As outlined below, various experimental polarization combinations, including circular, are needed to extract the pure symmetry components. A schematic figure of the experimental apparatus is given in Fig. 1. To ensure that the correct polarization is maintained in the sample, the incident light direction is normal to the sample surface. The polarization of the incident light is varied using a Soleil-Babinet (SB) compensator, which permits more convenient change of laser wavelength than do the usual $\frac{1}{4}$- and $\frac{1}{2}$-wave plates. The backscattered light is collected with $f/2.5$ optics, and im-

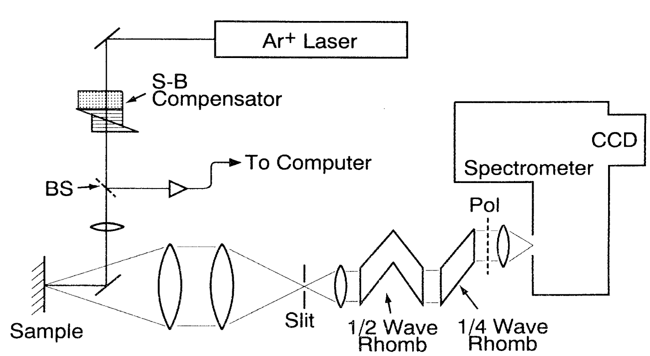

FIG. 1. Schematic of the apparatus used to obtain Raman spectra for various polarization combinations.

aged with 3× magnification onto the input slit of a Spex Triplemate spectrometer outfitted with a liquid-nitrogen–cooled charge-coupled-device (CCD) camera.

These measurements cover an extremely broad range of frequencies, since the inelastic scattering extends to energy shifts beyond 1 eV. The polarization analysis requires the conversion of circularly polarized light to linearly polarized light over this broad frequency range. This conversion is accomplished by $\frac{1}{2}$- and $\frac{1}{4}$-wave rhombs, which introduce relative phase differences of π and $\frac{1}{2}\pi$, respectively, between the electric-field components parallel and perpendicular to the plane of incidence of the rhomb. The dispersion in the phase shift introduced in the internal reflection in the rhombs is related to $dn/d\lambda$, which is small over the region of interest, and is not proportional to λ.

Since several spectra must be combined to extract the pure symmetry components, obtaining their correct magnitudes is essential. Consequently, during all scans, a photodiode monitors the laser power diverted by a beamsplitter (BS), and the spectra are normalized accordingly. The spectra are all calibrated to a standard lamp to correct for the response of the complete system, so that accurate line shapes may be obtained.

For the C_{4v} symmetry appropriate to the 2D CuO_2 planes, the Raman scattering tensor for electric-field vectors in the plane may be separated into four symmetry species: A_1, A_2, B_1, and B_2. Under the symmetry operations of C_{4v} these four representations transform like the polynomials x^2+y^2, x^3y-y^3x, x^2-y^2, and xy, respectively. In order to isolate all four of these symmetries, a variety of polarization combinations must be used, as indicated in Table I. The first column of this table indicates the symmetries contained in the scattering for the polarization combinations given in the second column. The first letter in the notation of the second column indicates the incident light polarization and the second letter indicates the scattered light polarization. As in our previous papers [1,3] x and y denote axes directed along the Cu-O bonds in the plane, while the x' and y' axes are rotated by 45° with respect to the x and y axes. R and L signify right and left circularly polarized light. Since there are twelve experimental polarization combinations available from which to determine four symmetry components, there are numerous consistency checks on the data.

TABLE I. Symmetries accessed with various combinations of incident and scattered light polarizations.

Symmetry	Geometry
A_1+B_1	xx, yy
A_2+B_2	xy, yx
A_1+B_2	$x'x'$, $y'y'$
A_2+B_1	$x'y'$, $y'x'$
A_1+A_2	RR, LL
B_1+B_2	RL, LR

The four independent symmetry components of the Raman scattering for a Gd_2CuO_4 sample using 4880 Å excitation are shown in Fig. 2. Note that the scattering persists to 8000 cm^{-1} (1 eV). The two features marked with asterisks in the A_1 scattering near 1560 and 2330 cm^{-1} are due to Raman scattering from atmospheric oxygen [11] and nitrogen [12], respectively, owing to the backscattering geometry employed. The other relatively sharp features below 800 and near 1200 cm^{-1}, which are not resolved, are due to single- [13] and two-phonon [14] scattering. The B_1 scattering, which arises from magnon pair creation, is well described by an effective interaction Hamiltonian involving nearest-neighbor sites [15]:

$$H_R = C\sum_{(ij)} (\mathbf{E}_{\rm inc}\cdot \boldsymbol{\sigma}_{ij})(\mathbf{E}_{\rm sc}\cdot \boldsymbol{\sigma}_{ij})\mathbf{S}_i\cdot\mathbf{S}_j\,, \qquad (1)$$

where $\mathbf{E}_{\rm inc}$ and $\mathbf{E}_{\rm sc}$ are electric-field vectors for the incident and scattering photons, and $\boldsymbol{\sigma}_{ij}$ is a unit vector connecting spin sites i and j. The matrix elements and other details of the excited-state exchange [16] determining H_R are contained in the prefactor C.

The spectrum calculated from Eq. (1) using noninteracting spin-wave theory is the two-magnon density of states (DOS) weighted by trigonometric form factors

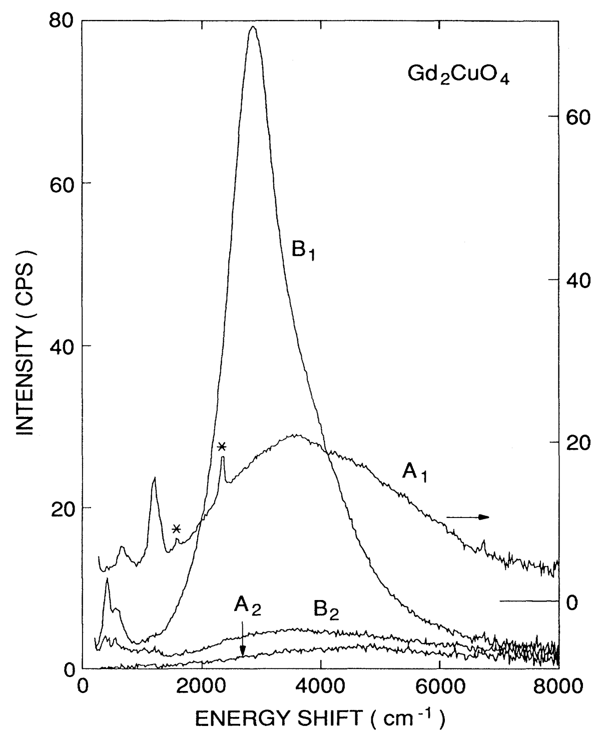

FIG. 2. The four pure symmetry components of the Raman scattering intensity vs energy shift for Gd_2CuO_4 taken with an incident laser wavelength of 4880 Å. The A_1 spectrum has been vertically offset for clarity; the asterisks mark Raman peaks from atmospheric N_2 and O_2.

which appear on transforming the real-space spin operators in Eq. (1) to k-space spin-wave operators. This spectrum diverges at twice the zone boundary magnon energy, which occurs at $4J$ for the CuO_2 planes, where J is the nearest-neighbor exchange energy in the 2D Heisenberg Hamiltonian. The two magnons created in the scattering event interact, however, leading to a broadening and shifting to lower energy of the peak in the spectrum. These magnon interaction effects may be accounted for with a proper Green-function calculation [17]. In particular, the spin-wave calculation including interaction effects [15] for a 2D Heisenberg antiferromagnet is in excellent agreement with the experimental data for K_2NiF_4 ($S=1$) [18]. An estimate of the effect of interactions on the scattering peak position may be obtained from a heuristic local Ising picture. In this picture, the scattering arises from flipping a pair of nearest-neighbor spins. Since six neighboring spins are parallel to the newly flipped spins, the energy of such a process should occur at $3J$, in reasonable agreement with the more sophisticated Green-function calculation.

For the spin-$\frac{1}{2}$ case, the line shape obtained from spin-wave theory is a factor of 3 narrower than the data for the B_1 symmetry shown in Fig. 2. The width of this B_1 feature is well accounted for by quantum spin fluctuations in the ground state of the spin-$\frac{1}{2}$ 2D Heisenberg Hamiltonian, as calculated using an Ising series-expansion technique [1], and confirmed by cluster [19] and Monte Carlo calculations [20].

The A_1 and B_2 scattering have been interpreted [1] within the Ising series expansion, using an effective scattering Hamiltonian involving diagonal next-neighbor (DNN) spin flips. The form of this Hamiltonian is the same as Eq. (1), with $\boldsymbol{\sigma}_{ij}$ replaced by a unit vector $\boldsymbol{\sigma}'_{ij}$ connecting a given site to a DNN site.

The scattering Hamiltonians introduced to describe the B_1, A_1, and B_2 scattering all appear naturally in a recent theory of Raman scattering in the Hubbard model [4]. In particular, Shastry and Shraiman find contributions to the scattering matrix element for the four symmetries of the form

$$O_{B_1}=\frac{t^2}{U-\omega}\sum_i \tfrac{1}{2}(\mathbf{S}_i\cdot\mathbf{S}_{i+y}-\mathbf{S}_i\cdot\mathbf{S}_{i+x}), \tag{2}$$

$$O_{A_1}=\frac{2t^4}{(U-\omega)^3}\sum_i(\mathbf{S}_i\cdot\mathbf{S}_{i+x+y}+\mathbf{S}_{i+x}\cdot\mathbf{S}_{i+y}+\cdots), \tag{3}$$

$$O_{B_2}=-\frac{4t^4}{(U-\omega)^3}\sum_i(\mathbf{S}_i\cdot\mathbf{S}_{i+x+y}-\mathbf{S}_{i+x}\cdot\mathbf{S}_{i+y}), \tag{4}$$

$$O_{A_2}=\frac{4t^4}{(U-\omega)^3}\sum_i\varepsilon_{\mu\mu'}\mathbf{S}_i\cdot(\mathbf{S}_{i+\mu}\times\mathbf{S}_{i+\mu'}), \tag{5}$$

where t is the hopping parameter, U is the on-site repulsion, $\mu=\pm x,\pm y$, and $\varepsilon_{\mu\nu}=-\varepsilon_{\nu\mu}=-\varepsilon_{-\mu\nu}$, and where terms of higher order in spin operator and terms beyond DNN have been suppressed. The B_1 contribution appears as the leading-order term in the $t/(U-\omega)$ expansion. The terms resulting in A_1 and B_2 scattering are higher order in the expansion, and for $\omega\ll U$ will be much weaker than the B_1 scattering. That these symmetries appear in the data of Fig. 2 indicates that we are near resonance. The matrix elements obtained from the expansion confirm the previous choice of scattering Hamiltonian [Eq. (1)]. The scattering of A_2 symmetry [Eq. (5)], however, is of a new type, and allows for the direct observation of dynamic fluctuations of the spin chirality.

While the A_2 scattering appears in the same order as the A_1 and B_2 in the $t/(U-\omega)$ expansion, the first nonvanishing contribution is of higher order in the spin-wave expansion. Specifically, the matrix element for scattering via the spin chirality term from the ground state to a two-magnon final state vanishes. Consider a general two-magnon final state, $|\psi\rangle$. Light scattering constrains the total momentum of this final state to zero; thus the momenta of the two magnons must be equal and opposite. Since the chirality operator, here denoted as $\hat{\chi}$, commutes with the total spin, S^z is preserved, forcing the two magnons to have oppositely directed spins. Thus the state $|\psi\rangle$ must be composed of a linear combination of states of the form $|+,k\rangle|-,-k\rangle$. Under the combined operations of time reversal, Θ, and a lattice translation, T, the ground state is even, as is this two-magnon state, $|\psi\rangle$. The spin chirality operator, however, is odd under these combined operations, leading to the conclusion that the matrix element, $\langle\psi|\hat{\chi}|0\rangle$, vanishes.

A spin-wave calculation for four noninteracting magnons yields an A_2 symmetry peak near $6.2J$, with a width (FWHM) $\sim 1.3J$ [21]. Interaction effects will reduce the energy of the peak position and may be estimated by the same heuristic local Ising picture adduced above to estimate the B_1 peak position near $3J$. In the case of the four-magnon contribution to the A_2 scattering, four spins in a row are flipped in a Néel ordered background [21]. This final configuration has ten nearest-neighbor spins parallel to the newly flipped spins, leading to an energy of $5J$. Figure 3, which compares the B_2 and A_2 on an expanded intensity scale, reveals that the spectral weight of the A_2 feature appears at a higher energy than that of the B_1 feature in Fig. 2, which peaks near 2870 cm^{-1}. The A_2 feature exhibits a broad peak centered near $\sim 5J$, with spectral weight extending to higher frequencies than the B_1 component, in qualitative agreement with the spin-wave estimate. Although this A_2 scattering intensity is small compared to the other symmetries, spectra taken with the 5145-Å Ar^+ laser line confirm the Raman nature of the feature. This A_2 symmetry scattering is also observed in very similar spectra for Pr_2CuO_4, as are the A_1, B_1, and B_2 features.

The four independent symmetries for the inelastic light scattering from the square lattice have been separately identified for Gd_2CuO_4 and Pr_2CuO_4. In addition to the previously identified spin fluctuation scattering in the B_1, A_1, and B_2 scattering channels, a new type of scattering

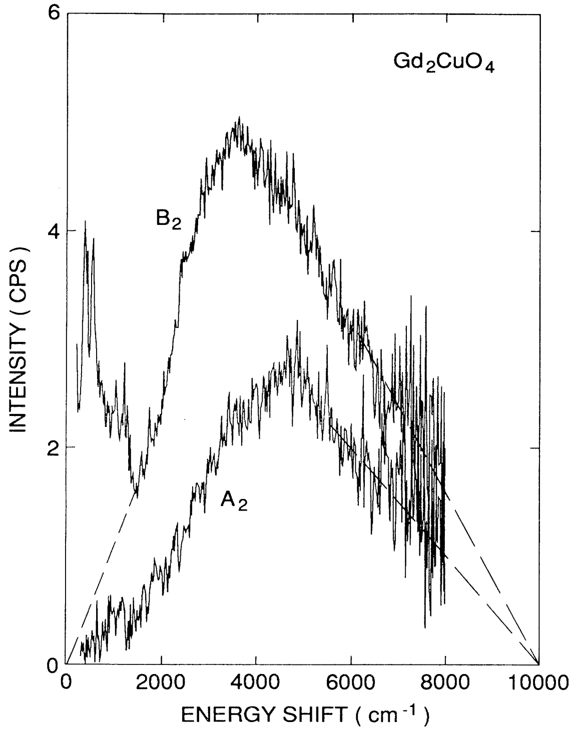

FIG. 3. Scattering intensity vs energy shift for the B_2 and A_2 symmetries of Gd_2CuO_4 taken with 4880-Å light on an expanded vertical scale. The dashed lines are guides to the eye which extrapolate the data linearly to zero.

corresponding to dynamic fluctuations of the spin chirality has been observed in the A_2 symmetry. This scattering comprises ~5% of the total integrated scattering intensity, and is very broad, extending beyond 1 eV. The position of this A_2 peak near $5J$ is in qualitative agreement with expectations based on spin-wave theory. More sophisticated calculations which include the effects of magnon interactions and quantum spin fluctuations are needed to obtain quantitative agreement with the data. These experimental results demonstrate that the Hubbard model accurately predicts the spin excitations of the insulating planar cuprates. Further experiments as a function of doping and temperature may clarify the nature and importance of chiral spin fluctuations in the doped planar cuprates.

We have greatly benefited from numerous helpful discussions with B. I. Shraiman and B. S. Shastry. We also thank S. J. Duclos and H. L. Carter for technical assistance.

[1] R. R. P. Singh, P. A. Fleury, K. B. Lyons, and P. E. Sulewski, Phys. Rev. Lett. **62**, 2736 (1989).

[2] K. B. Lyons *et al.*, Phys. Rev. B **39**, 9693 (1989).

[3] P. E. Sulewski *et al.*, Phys. Rev. B **41**, 225 (1990).

[4] B. S. Shastry and B. I. Shraiman, Phys. Rev. Lett. **65**, 1068 (1990); Int. J. Mod. Phys. B **5**, 365 (1991).

[5] X. G. Wen, F. Wilczek, and A. Zee, Phys. Rev. B **39**, 11413 (1989).

[6] Y. Chen, F. Wilczek, E. Witten, and B. Halperin, Int. J. Mod. Phys. B **3**, 1001 (1989); N. Nagaosa and P. A. Lee, Phys. Rev. Lett. **64**, 2450 (1990).

[7] N. Nagaosa and P. A. Lee, Phys. Rev. B **43**, 1233 (1991).

[8] R. B. Laughlin, Phys. Rev. Lett. **60**, 2677 (1988).

[9] S. L. Cooper *et al.*, Phys. Rev. B **42**, 10785 (1990).

[10] S-W. Cheong, J. D. Thompson, and Z. Fisk, Physica (Amsterdam) **158C**, 109 (1989).

[11] J. Bendtsen, J. Raman Spectrosc. **2**, 133 (1974).

[12] W. H. Fletcher and J. S. Rayside, J. Raman Spectrosc. **2**, 3 (1974).

[13] S. Sugai, T. Kobayashi, and J. Akimitsu, Phys. Rev. B **40**, 2686 (1989); E. T. Heyen *et al.*, Solid State Commun. **74**, 1299 (1990).

[14] C. Thomsen, E. Schönherr, B. Friedl, and M. Cardona, Phys. Rev. B **42**, 943 (1990).

[15] J. B. Parkinson, J. Phys. C **2**, 2012 (1969).

[16] P. A. Fleury and R. Loudon, Phys. Rev. **166**, 514 (1968).

[17] R. J. Elliot and M. F. Thorpe, J. Phys. C **2**, 1630 (1969).

[18] P. A. Fleury and H. J. Guggenheim, Phys. Rev. Lett. **24**, 1346 (1970).

[19] E. Gagliano and S. Bacci, Phys. Rev. B **42**, 8772 (1990); E. Dagotto and D. Poilblanc, Phys. Rev. B **42**, 7940 (1990).

[20] Z. Liu and E. Manousakis, Phys. Rev. B **43**, 13246 (1991).

[21] B. I. Shraiman and B. S. Shastry (unpublished).